# Supplementary Information (SI)

## *In Situ* Self-Assembly of Amine-Rich Carbon Supraparticles for Rapid $CO_2$ Captures

*Jinglin He,[#ab] Ziheng Jin,[#a] Rui Zhou,[a] Zhongde Dai,[a] Hui Su,[a] Yiqiao Zhang,[a] Bangda Wang,[a] Xia Jiang*[a]*

[a]. College of carbon neutrality future technology, Sichuan university, Chengdu 610065, China.

[b]. College of architecture & environment, Sichuan university, Chengdu 610065, China.

[#]Both authors contributed equally to this article.

Xia Jiang, Professor

Tel: 86-13688330205

Email: xjiang@scu.edu.cn

# Table of contents

**Characterization of amino-functionalized CSs** 1
**$CO_2$ Adsorption Performance** 2
**Calculation of performance indicators** 3
**Figure S1**. pH assessment of amine-functionalized CSs after water soaking. ....7
**Figure S2**. Thermogravimetric (TG/DTG) analysis of amine. ....8
**Figure S3**. Stepwise $N_2$–TG volatilization profiles of PEI- and TEPA-functionalized CSs. ....9
**Figure S4**. the C1s and O1s spectra of CSs. ....10
**Figure S5.** the O1s spectra of amine-functionalized CSs. ....11
**Figure S6.** the C1s spectra of amine-functionalized CSs. ....12
**Figure S7.** the N1s spectra of amine-functionalized CSs. ....13
**Figure S8.** FTIR spectra of CSs and amine-functionalized CSs. ....14
**Figure S9.** SEM image and corresponding EDS mapping of the sample cross-section. ....15
**Figure S10.** Mercury intrusion and extrusion curves (cumulative intrusion volume vs pressure) of (a) PEI-CSs(P), (b) PEI-CSs(I), (c) TEPA-CSs(P), and (d) TEPA-CSs(I). ....16
**Figure S11.** $N_2$ adsorption and desorption curves of (a)PC-K-1CNF (b) PEI functionalized CSs (c) TEPA functionalized CSs. ....17
**Figure S12.** Meso- and macro- pore size distribution of (a) PEI functionalized CSs (b) TEPA functionalized CSs. ....18
**Figure S13.** Cumulative pore volume loss within the pore size ranges of (a) 0-2 nm and (b) 2 – 100 nm, with PEI-functionalized CSs shown in yellow and TEPA-functionalized CSs shown in purple. ....19
**Figure S14.** $CO_2$ adsorption capacity at 70 °C of in situ TEPA-functionalized CSs with different TEPA loadings. ....20
**Figure S15.** FTIR spectra of (a) CSs-PEI(I), (b) CSs-TEPA(I) (c) CSs-PEI(P) and (d) CSs-TEPA(P) before and after 10 adsorption – desorption cycles. ....21
**Figure S16.** $N_2$ adsorption–desorption isotherms of (a) CSs-TEPA(I) and (b) CSs-PEI(I) before and after 10 adsorption–desorption cycles. ....22
**Figure S17.** SEM mapping of the microstructure of PC-K-1CNF. ....23
**Figure S18.** Multi-model kinetic analysis of $CO_2$ uptake on amine-functionalized CSs. ....24
**Figure S19.** Pseudo-second-order model on normalized $CO_2$ adsorption curves at 70°C of (a) PEI functionalized CSs and (b)TEPA functionalized CSs. ....25
**Figure S20.** $CO_2$ adsorption curves of TEPA-CSs(I) at 70 °C under 15 vol% $CO_2$/85 vol% $N_2$, with $\tau_{90}$ and average adsorption rates indicated. ....26
**Figure S21.** A nonlinear regression analysis of mesopore volume versus $\tau$ 90. ....27

**Table S1.** Content analysis of C, H and N elements and actual load calculation of amine-functionalized CSs. ....28
**Table S2.** Total nitrogen (TN) concentration in soaking solutions after water soaking of amine-functionalized CSs. ....29
**Table S3.** Adsorption heat and desorption energy consumption. ....30
**Table S4.** Comparisons with Existing Studies ....31

**Characterization of amino-functionalized CSs**

The external surface and internal morphology of the samples were examined using a field emission scanning electron microscope (SEM, Hitachi High-tech Regulus 8220, Japan). Elemental analyses for carbon, hydrogen, and nitrogen were performed with a Vario EL Cube elemental analyzer (EA, Elemental, Germany), which offers a precision of <0.1% for C, H, and N. X-ray photoelectron spectroscopy (XPS, Thermo Scientific K-Alpha™, USA) was employed to analyze surface chemical states, using a monochromatic Al Kα X-ray source (hν = 1486.6 eV). Fourier transform infrared (FTIR) spectra were recorded on a PerkinElmer spectrometer equipped with an ATR accessory. Spectra were collected in the range 4000–600 $cm^{-1}$ with a resolution of 4 $cm^{-1}$ by co-adding 32 scans. The elemental compositions of C, O, and N on the surface of the samples were directly determined by energy-dispersive X-ray spectroscopy (EDS, FEI Nova nanoSEM 450, USA). Thermogravimetric (TG) and derivative thermogravimetric (DTG) analyses were carried out using a STA800 synchronous thermal analyzer (PerkinElmer, USA). The measurements were conducted under a flow of high-purity $N_2$ (99.99%) at 50 mL/min with a heating rate of 10 °C/min up to 800 °C, and the maximum weight loss peak was determined from the derivative curve. The specific surface area and pore structure of the samples were determined using a surface area and porosity analyzer (Micromeritics ASAP 2460, USA). Before measurement, about 100 mg of sample was degassed at 120 °C for 8 h under vacuum (< 50 mTorr). $N_2$ adsorption–desorption isotherms were recorded at −196 °C using liquid nitrogen. Macropore size distribution ($V_{macro}$) was determined by an automatic mercury intrusion porosimeter (MIP, Micromeritics AutoPoreIV 9500, USA). The measurements were conducted progressively in the pressure range from 0.1 psi to 61,000 psi corresponding to a pore diameter from 5 nm to 350 μm.

**$CO_2$ Adsorption Performance**

The $CO_2$ adsorption capacity was measured using a simultaneous thermal analyzer (PerkinElmer STA 8000, USA). Pure $CO_2$ was used to evaluate the intrinsic $CO_2$ uptake of the sorbents, while the 15 vol% $CO_2$/85 vol% $N_2$ mixture was selected as a surrogate post-combustion flue gas composition[1]. For the adsorption step, the samples were first heated to 120 °C at 5 °C $min^{-1}$ under $N_2$ (50 mL $min^{-1}$) and held for 30 min to ensure complete outgassing. The system was then cooled to the target adsorption temperature (30, 50, 70, 100, or 120 °C), after which the inlet gas was switched to either pure $CO_2$ (50 mL $min^{-1}$) or a 15 vol% $CO_2$/85 vol% $N_2$ mixture (50 mL $min^{-1}$). Among these temperatures, 70 °C lies within a practically relevant window for medium-temperature post-combustion $CO_2$ capture and was therefore chosen as the reference condition for detailed kinetic and cyclic adsorption–desorption experiments. The adsorption heat and desorption energy consumption during $CO_2$ release were evaluated by differential scanning calorimetry (DSC) integrated into the thermal analyzer. The $CO_2$ adsorption capacity, expressed in mmol $g^{-1}$, was determined from the sample mass change during the adsorption phase, and the cyclic adsorption performance was assessed by repeating the procedure for 10 consecutive cycles.

**Calculation of performance indicators:**

(1) The BET surface area ($S_{BET}$) was calculated from the linear part of the BET plot in the relative pressure ($P/P_0$) range of 0.01–0.30. The total pore volume ($V_{tot}$) was estimated from the amount of $N_2$ adsorbed at $P/P_0 \approx 0.99$. The t-plot method ($P/P_0$ = 0.10–0.20) was used to estimate the micropore volume ($V_{mic}$), and the mesopore volume ($V_{meso}$) and pore size distribution were obtained from the adsorption branch using the BJH model.

(2) For the analysis of cumulative pore volume loss, the pore size distributions obtained from the BJH model were further processed. The cumulative pore volume within a given pore-size window (2–20 nm, 2–50 nm, or 2–100 nm) was calculated by integrating the BJH pore volume distribution over the corresponding diameter range. The pore volume loss ($\Delta V$, $cm^3\ g^{-1}$) was calculated according to the following equation:

$$\Delta V = V_{cum,CSs} - V_{cum,amine\ sample} \quad \text{..... (1)}$$

where $V_{cum,CSs}$ is the cumulative pore volume of the pristine CSs within the specified pore-size range, and $V_{cum,amine\ sample}$ is the cumulative pore volume of the corresponding amine-functionalized sample within the same range.

The resulting $\Delta V$ values were plotted as a function of amine loading, as determined from elemental analysis (**Table S1,** EA), in **Figure 4e,f and Figure S9**.

(3) $CO_2$ adsorption capacity/ $CO_2$ uptake

The equilibrium $CO_2$ adsorption capacity ($A_{CO_2}$, $mmol\ g^{-1}$) obtained from TGA was calculated from the mass gain of the sorbent according to:

$$A_{CO_2} = \frac{\Delta m}{44 * m_0} \quad \text{..... (2)}$$

where $\Delta m$ (g) is the mass increase during $CO_2$ adsorption, $m_0$ (g) is the initial dry mass of the sorbent, and 44 is the molar mass of $CO_2$ ($g\ mol^{-1}$).

(4) Amine utilization efficiency ($\eta$, %) was calculated according to the following equation:

$$\eta = \frac{A_{CO_2}}{N_{amine}} \times 100\%$$

..... (3)

where $A_{CO_2}$ is the $CO_2$ adsorption capacity (mmol/g) and $N_{amine}$ is the amine group content, was quantified by CHN elemental analysis and expressed as millimoles of nitrogen per gram of dry sorbent (mmol N $g^{-1}$).

(5) $\tau_{90}/\tau_{80}$: Time to reach 90% and 80% of equilibrium uptake ($\tau_{90}$, $\tau_{80}$)

(6) Average adsorption rate up to 80% uptake

The average adsorption rate up to 80% of the equilibrium capacity ($\bar{R}_{80}$, mmol $g^{-1}$ $min^{-1}$) was calculated as:

$$\bar{R}_{80} = (0.80 * A_{CO_2})/\tau_{80}$$

..... (4)

(7) Peak adsorption rate

The peak adsorption rate ($R_{peak}$, mmol $g^{-1}$ $min^{-1}$) was obtained from the $CO_2$ uptake–time curves at 70 °C under 100 vol% $CO_2$ (**Figure 6e,f**) according to:

$$R_{peak} = \max_t (d A_{CO_2}/dt)$$

..... (5)

(8) $\iint_{Time}^{DTG} 3$

The percentage of $CO_2$ uptake achievable within the first 3 min was determined by integrating the DTG curve over this time interval.

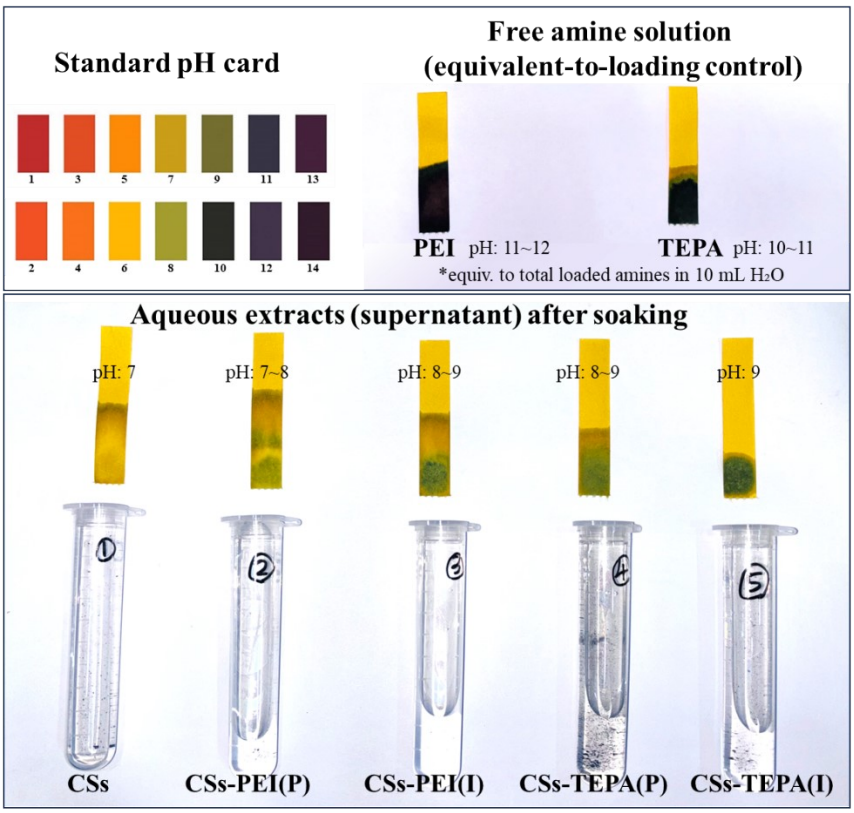


**Figure S1**. pH assessment of amine-functionalized CSs after water soaking.

**Note:** To qualitatively evaluate post-synthesis amine leaching, each sample (0.10 g; CSs, CSs-PEI(P), CSs-PEI(I), CSs-TEPA(P), or CSs-TEPA(I)) was dispersed in deionized water (10 mL) and shaken at room temperature for 1 h. The suspensions were then allowed to settle (or briefly centrifuged), and the supernatants (aqueous extracts) were collected. The pH of each extract was assessed using a standard pH indicator strip/card and recorded by comparison with the reference color scale. As free-amine controls, aqueous PEI and TEPA solutions containing an equivalent total amine mass to the corresponding loaded amount were prepared in 10 mL water and measured under the same conditions. The total nitrogen (TN) concentrations in the aqueous extracts are summarized in **Table S2**.

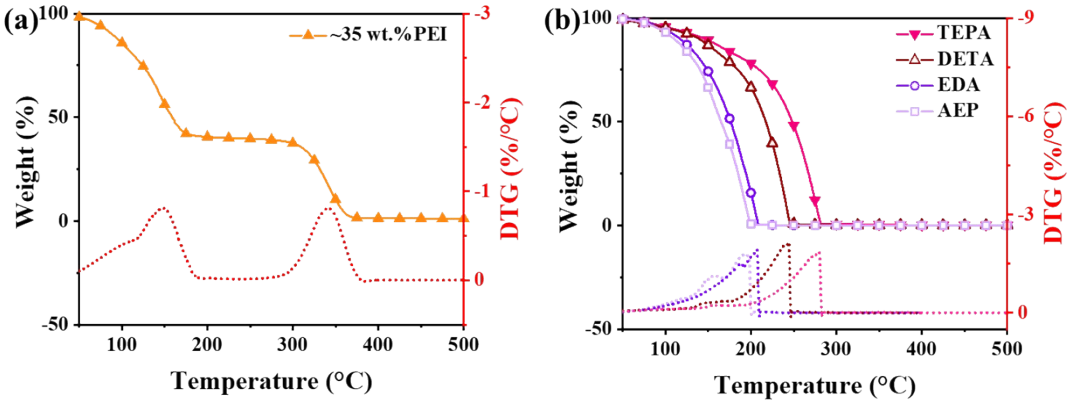


**Figure S2**. Thermogravimetric (TG/DTG) analysis of amine.

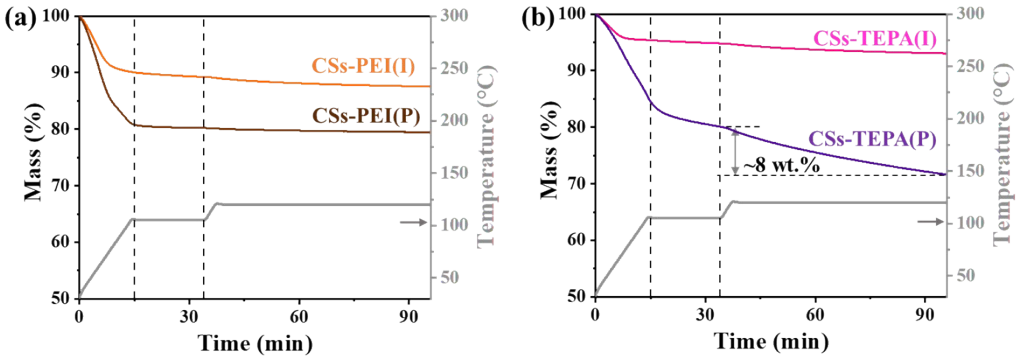


**Figure S3**. Stepwise $N_2$–TG volatilization profiles of PEI- and TEPA-functionalized CSs.

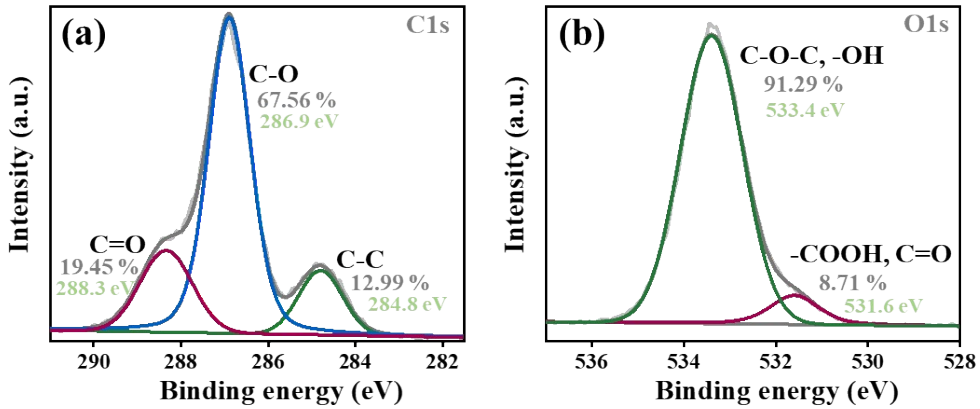


**Figure S4**. the C1s and O1s spectra of CSs.

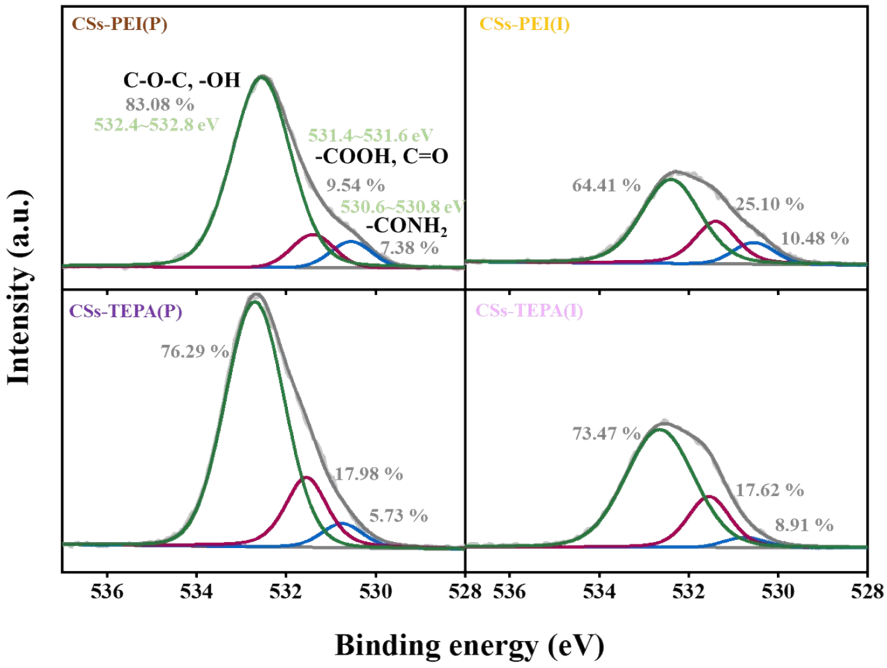


**Figure S5.** the O1s spectra of amine-functionalized CSs.

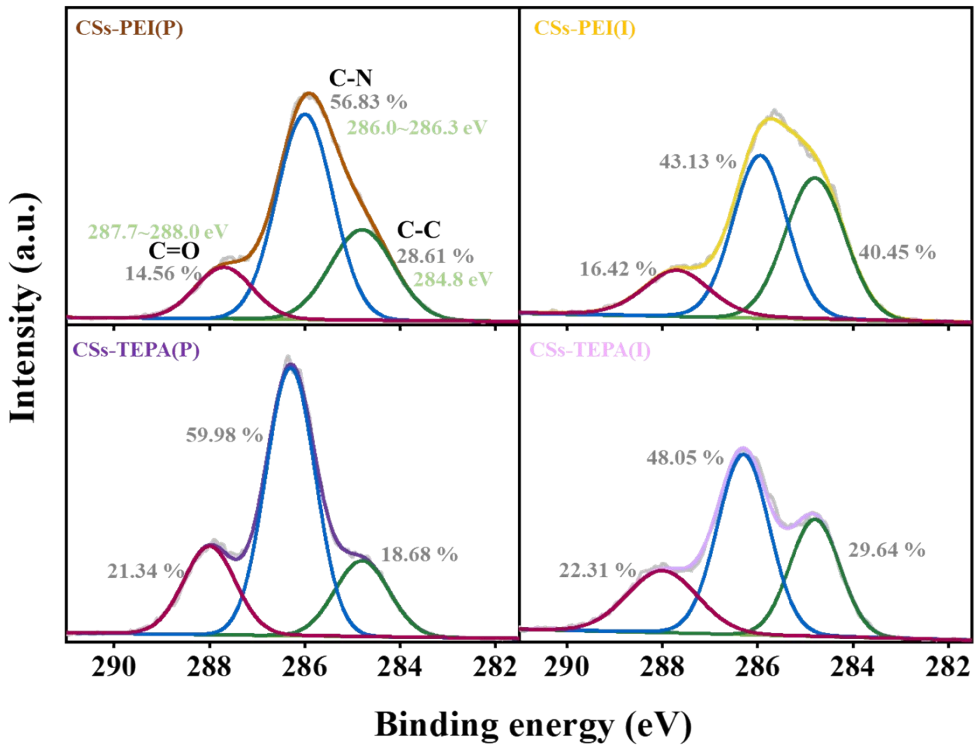


**Figure S6.** the C1s spectra of amine-functionalized CSs.

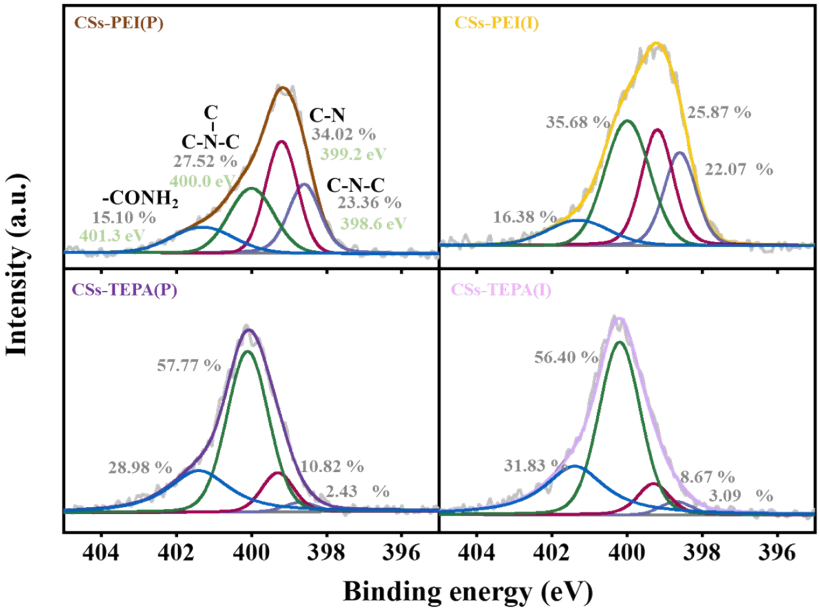


**Figure S7.** the N1s spectra of amine-functionalized CSs.

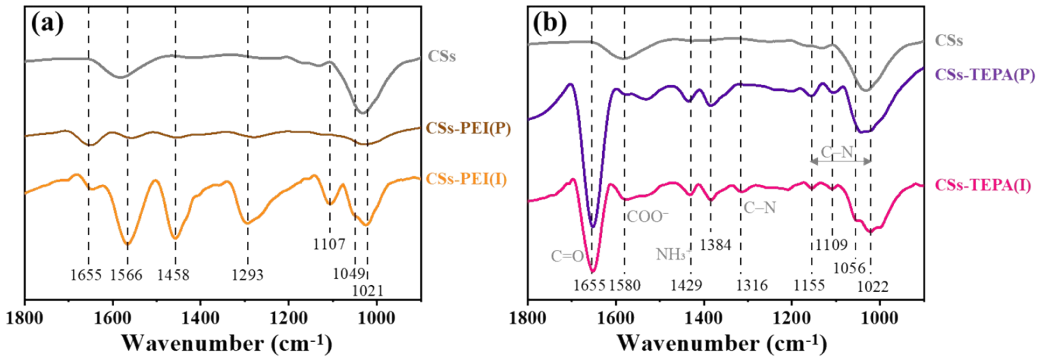


**Figure S8.** FTIR spectra of CSs and amine-functionalized CSs.

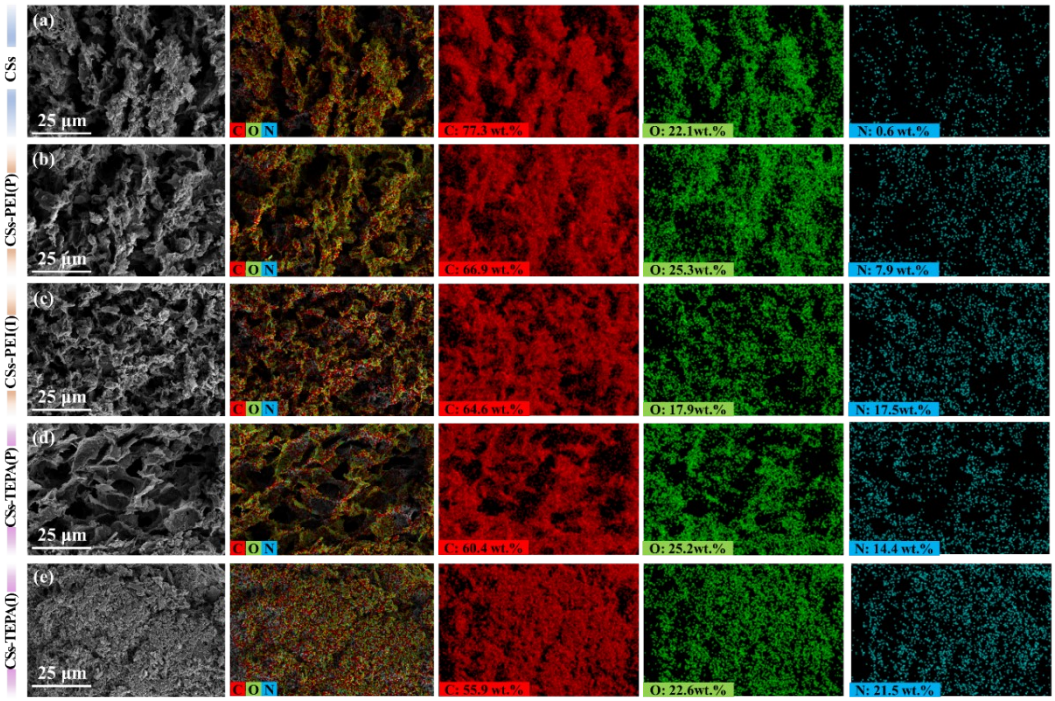


**Figure S9.** SEM image and corresponding EDS mapping of the sample cross-section.

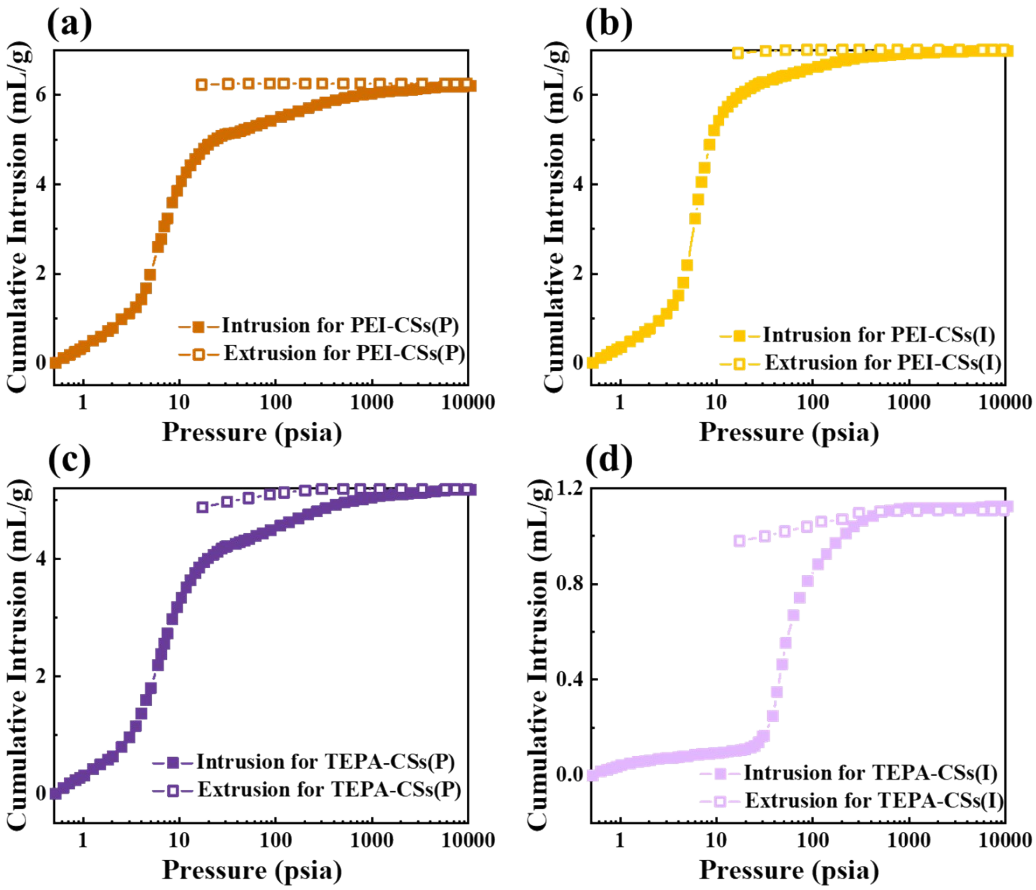


**Figure S10.** Mercury intrusion and extrusion curves (cumulative intrusion volume vs pressure) of (a) PEI-CSs(P), (b) PEI-CSs(I), (c) TEPA-CSs(P), and (d) TEPA-CSs(I).

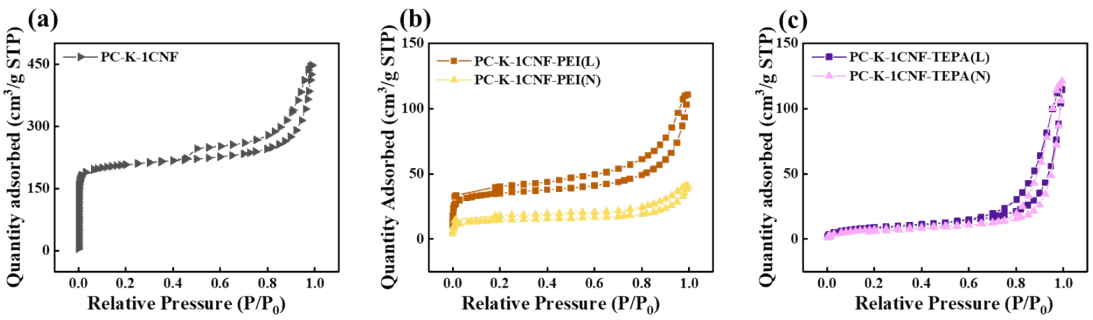


**Figure S11.** $N_2$ adsorption and desorption curves of (a)PC-K-1CNF (b) PEI functionalized CSs (c) TEPA functionalized CSs.

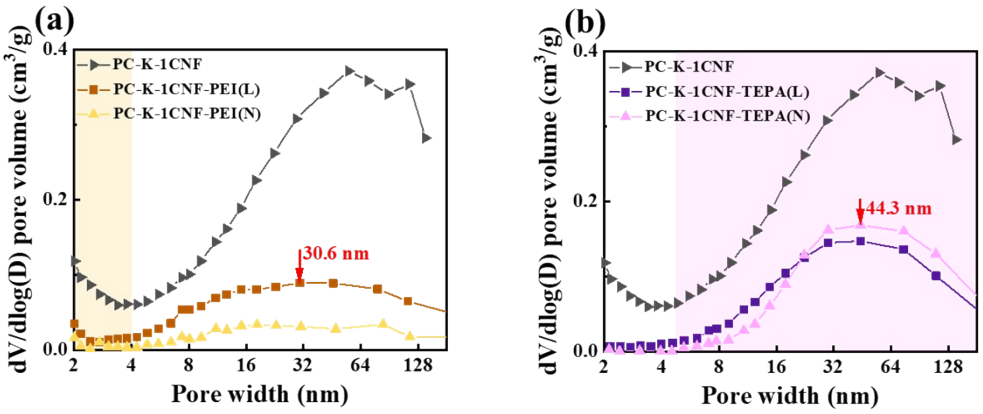


**Figure S12.** Meso- and macro- pore size distribution of (a) PEI functionalized CSs (b) TEPA functionalized CSs.

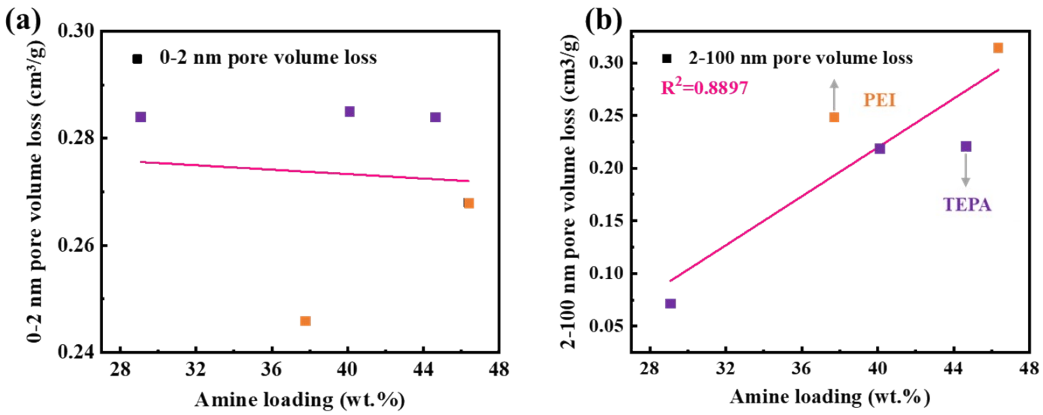


**Figure S13.** Cumulative pore volume loss within the pore size ranges of (a) 0-2 nm and (b) 2–100 nm, with PEI-functionalized CSs shown in yellow and TEPA-functionalized CSs shown in purple.

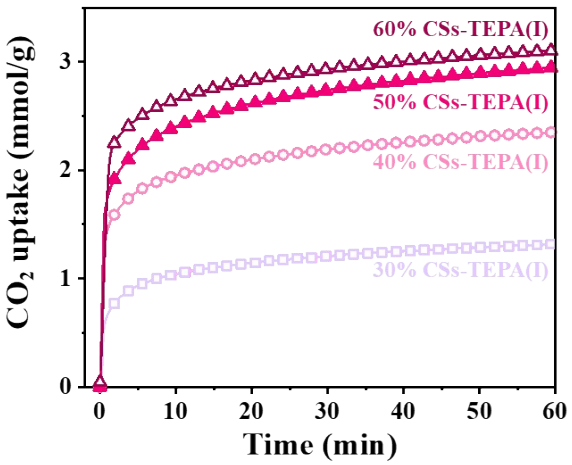


**Figure S14.** $CO_2$ adsorption capacity at 70 °C of in situ TEPA-functionalized CSs with different TEPA loadings.

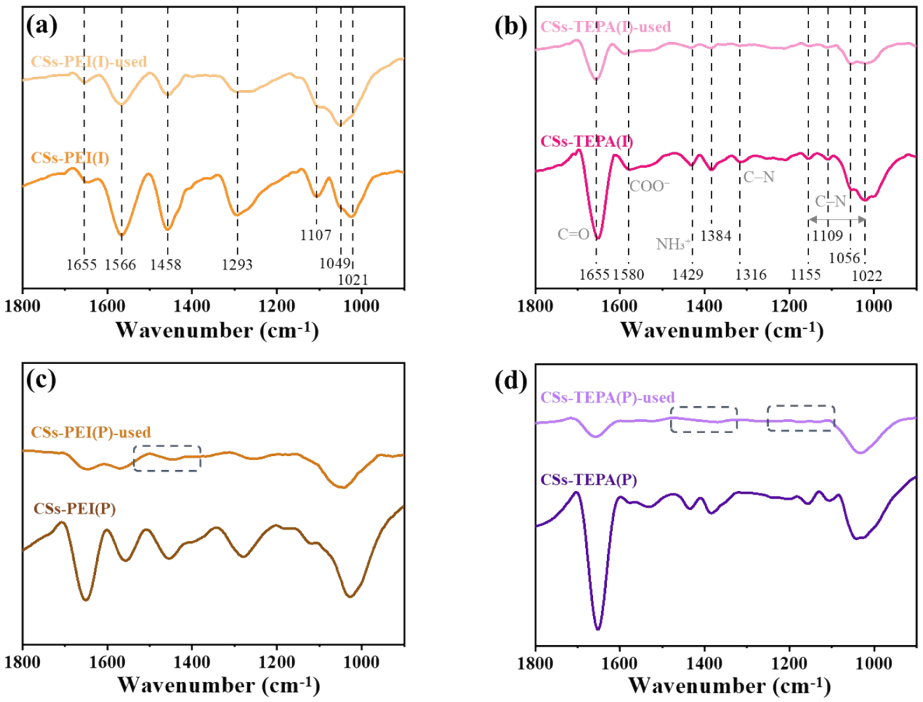


**Figure S15.** FTIR spectra of (a) CSs-PEI(I), (b) CSs-TEPA(I) (c) CSs-PEI(P) and (d) CSs-TEPA(P) before and after 10 adsorption–desorption cycles.

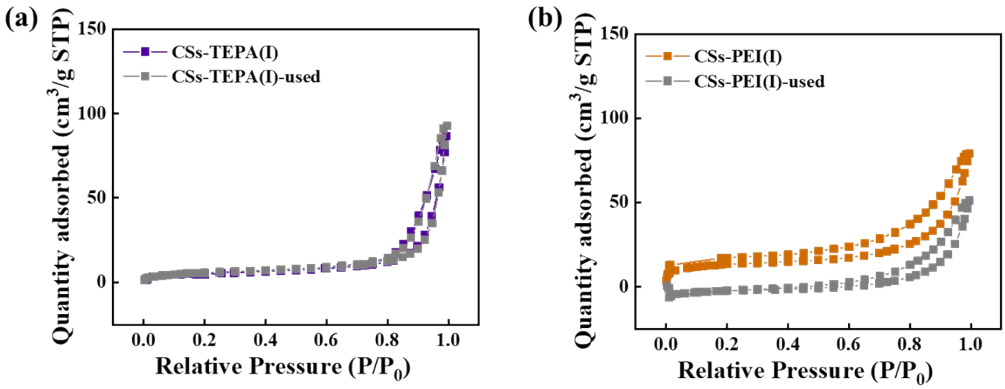


**Figure S16.** $N_2$ adsorption–desorption isotherms of (a) CSs-TEPA(I) and (b) CSs-PEI(I) before and after 10 adsorption–desorption cycles.

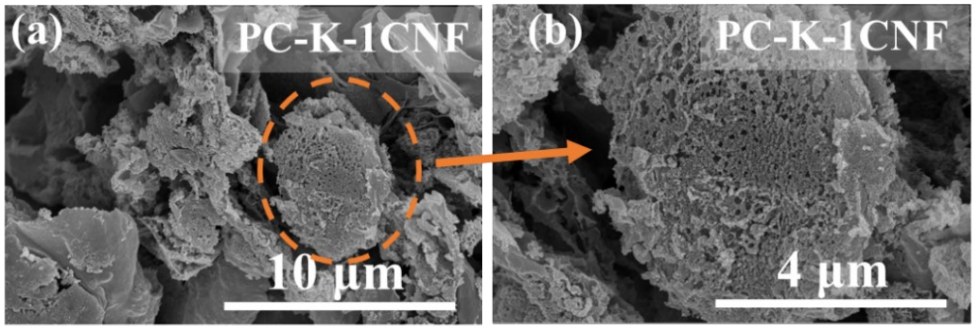


**Figure S17.** SEM mapping of the microstructure of PC-K-1CNF.

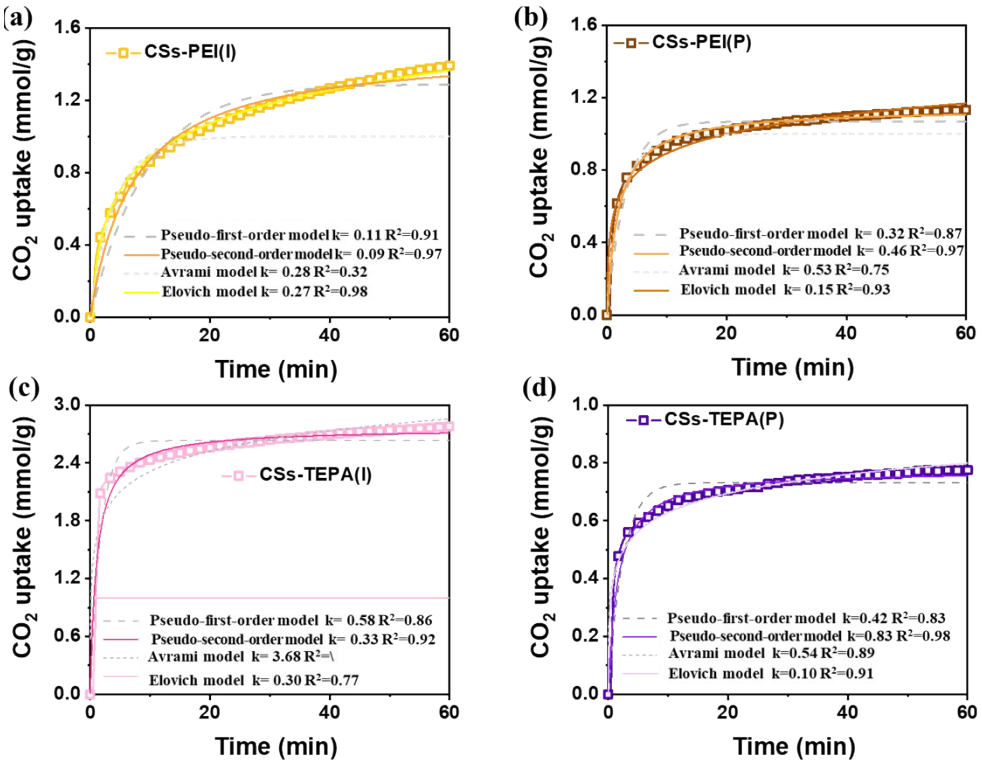


**Figure S18.** Multi-model kinetic analysis of $CO_2$ uptake on amine-functionalized CSs.

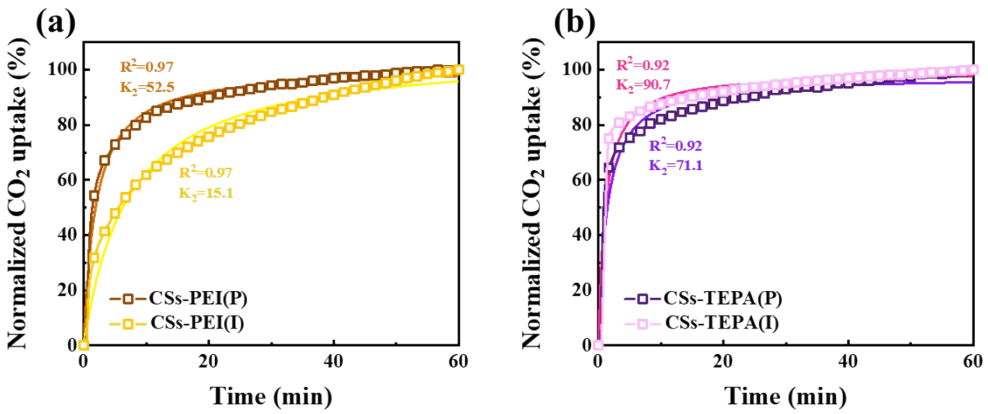


**Figure S19.** Pseudo-second-order model on normalized $CO_2$ adsorption curves at 70°C of (a) PEI functionalized CSs and (b)TEPA functionalized CSs.

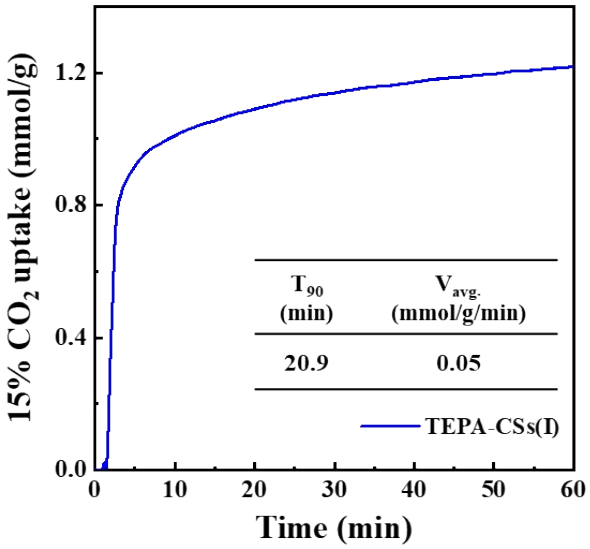


**Figure S20.** $CO_2$ adsorption curves of TEPA-CSs(I) at 70 °C under 15 vol% $CO_2$/85 vol% $N_2$, with $\tau_{90}$ and average adsorption rates indicated.

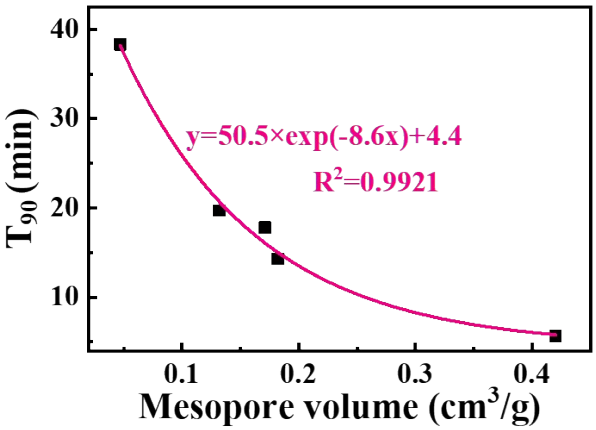


**Figure S21.** A nonlinear regression analysis of mesopore volume versus τ90.

**Table S1.** Content analysis of C, H and N elements and actual load calculation of amine-functionalized CSs.

| Sample | Content of elements（wt.%） | | | Actual amine loading/grafting amount（wt.%） | |
|---|---|---|---|---|---|
| | N | C | H | Based EA[1] | Based TG[2] |
| CSs | 1.24 | 66.29 | 2.90 | \ | \ |
| CSs-PEI(P) | 15.08 | 60.42 | 6.20 | 44.2 | 42.6 |
| CSs -PEI(I) | 15.76 | 54.21 | 7.51 | 46.4 | 49.1 |
| CSs -TEPA(P) | 16.09 | 59.58 | 5.27 | 41.5 | 42.0 |
| CSs -TEPA(I) | 17.21 | 48.86 | 6.88 | 44.6 | 48.5 |
| Spent CSs -PEI(P) | 15.96 | 64.69 | 5.65 | 47.0 | - |
| Spent CSs -PEI(I) | 16.92 | 63.9 | 6.24 | 50.1 | - |
| Spent CSs -TEPA(P) | 15.59 | 60.9 | 4.91 | 40.1 | - |
| Spent CSs -TEPA(I) | 18.01 | 56.87 | 6.61 | 46.9 | - |

Note：

1. Calculate the mass percentage of the amine groups using the nitrogen content. Assuming that the nitrogen element is entirely derived from the amine groups, determine the molar ratio between the nitrogen element and the amine groups based on the chemical formula of the amine groups.

$$\text{Amine Loading (wt.\%)} = \frac{N\ wt.\% \times Tehe\ molar\ mass\ of\ amine\ groups}{The\ molar\ mass\ of\ nitrogen\ in\ the\ amine\ group} \times 100\%$$

2. Determine the weight loss percentage (ΔW) in the 150–400°C range, attributed to amine group decomposition. Using the initial sample mass ($M_0$), calculate amine loading as:

$$\text{Amine Loading (wt.\%)} = \frac{\Delta M}{M_0} \times 100\%$$

This assumes the weight loss is solely due to amine decomposition.

The density of PEI used in the experiment is 1.03 g·cm$^{-3}$, so the theoretical maximum load of the original superparticle carbon ball matrix pore is：

$$（1.03\times0.692）/（1.03\times0.692+1）=42\ \text{wt.\%} \quad \text{(S1)}$$

**Table S2.** Total nitrogen (TN) concentration in soaking solutions after water soaking of amine-functionalized CSs.

| **Sample**<br>(soaking solution after water soaking) | **TN concentration**<br>ρ(TN) (mg $L^{-1}$) |
|---|---|
| CSs | 0.038 |
| **PEI**<br>the corresponding free-amine solutions | **442.316** |
| CSs-PEI(P) | 35.242 |
| CSs-PEI(I) | 23.916 |
| **TEPA**<br>the corresponding free-amine solutions | **672.842** |
| CSs-TEPA(P) | 231.411 |
| CSs-TEPA(I) | 169.558 |

**Table S3.** Adsorption heat and desorption energy consumption.

| Sample | Adsorption heat ΔHr [kJ·mol $_{CO2}^{-1}$] | Desorption energy consumption Q [kJ·mol $_{CO2}^{-1}$] |
|---|---|---|
| CSs[a] | 18.70 | 13.89 |
| CSs-PEI(P)[b] | 49.18 | 66.26 |
| CSs-PEI(I)[b] | 33.14 | 55.09 |
| CSs-TEPA(P)[b] | 40.80 | 89.27 |
| CSs-TEPA(I)[b] | 63.17 | 92.01 |

Note:

a: The operating conditions of adsorption and desorption were 30 min at 30°C and 30 min at 120°C, respectively.

b: The operating conditions of adsorption and desorption were 70°C for 60 min and 120°C for 30 min, respectively.

**1. Adsorption heat ($\triangle H_r$)**

During the adsorption step, the heat-flow data were corrected by subtracting the blank (empty-pan) baseline. The net heat released during adsorption was calculated by integrating the baseline-corrected heat-flow curve:

$$Q_{ads} = \int (\emptyset_{sample} - \emptyset_{blank}) dt$$

The adsorption heat per mole of $CO_2$ was then calculated as:

$$\triangle H_r = \frac{Q_{ads}}{n_{CO_2}}$$

Where $n_{CO_2}$ is the amount of $CO_2$ adsorbed, mol; A positive $\triangle H_r$ indicates exothermic adsorption, kJ·mol $_{CO2}^{-1}$

**2. Desorption energy consumption (Q)**

The total energy required for desorption includes the energy needed to heat the sample from the adsorption temperature to 120 °C ($Q_{heat}$), and the heat-flow signal associated with $CO_2$ desorption ($Q_{des}$), kJ·mol $_{CO2}^{-1}$:

$$Q_{heat} = C_{totle}(T_{des} - T_{ads})$$

$$Q_{des} = \int (\emptyset_{des} - \emptyset_{blank}) dt$$

The total desorption energy per mole of $CO_2$ is:

$$Q = \frac{Q_{heat} + Q_{des}}{n_{CO_2}}$$

**Table S4.** Comparisons with Existing Studies

| Material type | Porous structure | | | Amine payload and method (wt%) | Amine efficiency (mmol $CO_2$/mmol N %) | $CO_2$ adsorption capacity (mmol/g) | Adsorption heat ($kJ \cdot mol_{CO2}^{-1}$) | $t_{80\%}$ | Deactivation rate per cycle | Ref |
|---|---|---|---|---|---|---|---|---|---|---|
| | $S_{BET}$ ($m^2/g$) | V ($cm^3/g$) | $V_{ave.}$ (nm) | | | | | | | |
| Silica | 267[b] | - | - | PEI: 30.0, post load | 19 | 1.7 Weight method (100% CO2 at 25 °C) | - | - | - | [2] |
| Silica | 195[b] | 0.39[b] | 6[b] | PEI: -, post load | - | 0.9 Weight method (100% $CO_2$ at 25 °C) | - | 19.2 min | - | [3] |
| Silica | 502[b] | 5.46[b] | - | PEI: 56.5, post load | 33 | 4.3 Weight method (100% $CO_2$ at 75 °C) | - | 5.5 min | 1.70% | [4] |
| Silica | 156[b] | 0.84[b] | - | PEI: 51.7, post load | 27 | 3.2 Weight method (100% $CO_2$ at 25 °C) | - | ~10 h | - | [5] |
| Silica | 54[b] | 0.05[b] | 4[b] | TEPA: 75.0, post load | 28 | 5.6 Weight method | 49.5 | - | 1.90% | [6] |

| | | | | | | | | | | |
|---|---|---|---|---|---|---|---|---|---|---|
| | | | | | | (100% $CO_2$ at 70 °C) | | | | |
| Silica | 261[a] | 1.81[a] | 10-15[a] | PEI: 50.0, post load | - | 3.7 Weight method (15% $CO_2$ and 3% $H_2O$ in $N_2$ balance at 40 °C) | 177.3 | - | ~10.00% (14 days) | [7] |
| Silica | 4[b] | 0.06[b] | - | TEPA: 70.0, post load | 31 | 5.8 Weight method (15% $CO_2$ in $N_2$ balance at 75 °C) | - | 13 min | 6.90% | [8] |
| Silica | 54[b] | 0.48[b] | 23[b] | TEPA: 50.0, post load | 38 | 5.1 Weight method (15% $CO_2$ in $N_2$ balance at 75 °C) | - | - | 0.69% | [9] |
| Silica | 14[b] | 0.08[b] | 18[b] | PEI: 40.0, post load | - | 2.3 Weight method (15% $CO_2$ in $N_2$ balance at 75 °C) | 56.0 | ~4 min | - | [10] |

| | | | | | | | | | | |
|---|---|---|---|---|---|---|---|---|---|---|
| $Al_2O_3$ | 388[a] | 1.61[a] | 13.1[a] | PEI: 60.0, post load | 29 | 4.3 Weight method (100% $CO_2$ at 90 °C) | - | 4 min | 0.14 % | [11] |
| Polymer | 117[b] | 0.40[b] | 13[b] | Mixed amine:-, in-situ grafting | 48 | 2.1 Weight method (100% $CO_2$ at 75 °C) | - | 22 min | - | [12] |
| Polymer | 149[b] | - | - | PEI: -, post load | - | 6.5 Volume method (100% $CO_2$ at 25 °C) | - | - | 1.54% | [13] |
| Polymer | 335[b] | 60.3[b] | 3[b] | Phthalimide: 60.0, in-situ grafting | - | 7.1 Volume method (100% $CO_2$ at 25 °C) | - | ~3h | - | [14] |
| Polymer | 234[b] | - | - | PEI: 50, post load | - | 1.7 Weight method (100% $CO_2$ at 75 °C) | - | ~2 min | 0.70% | [15] |
| CSs | 27[b] | 1.3[b] | 27.5[b] | TEPA:48.5, in-situ grafting | 49 | 2.9 Weight method (100% $CO_2$ at 75 °C) | 92.0 | ~2.5 min | 1.03% | This work |

Note: [a] Pore structure of the pristine support. [b] Pore structure of the sorbents after amine functionalization.

## Reference


1 H. Ghaedi, J. Fu, P. Kalhor, S. M. Soltani and M. Zhao, *J. Mater. Chem. A*, 2025, **13**, 23655–23670.

2 E. Vilarrasa-Garcia, E. M. O. Moya, J. A. Cecilia, C. L. Cavalcante, J. Jiménez-Jiménez, D. C. S. Azevedo and E. Rodríguez-Castellón, *Micropor. Mesopor. Mat.*, 2015, **209**, 172–183.

3 K. Sim, N. Lee, J. Kim, E.-B. Cho, C. Gunathilake and M. Jaroniec, *ACS Appl. Mater. Interfaces*, 2015, **7**, 6792−6802.

4 Y. Han, G. Hwang, H. Kim, B. Z. Haznedaroglu and B. Lee, *Chem. Eng. J.*, 2015, **259**, 653–662.

5 E. A. Chernikova, L. M. Glukhov, V. G. Krasovskiy, G. I. Kapustin, N. A. Davshan, I. V. Mishin and L. M. Kustov, *Micropor. Mesopor. Mat.*, 2025, **394**, 113680.

6 H. Yan, G. Zhang, Y. Xu, Q. Zhang, J. Liu, G. Li, Y. Zhao, Y. Wang and Y. Zhang, *Fuel*, 2022, **315**, 123195.

7 C. Kim, Y. Ha and M. Choi, *Acc. Chem. Res.*, 2023, **56**, 2887–2897.

8 P. Zhao, G. Zhang, Y. Xu and Y. Lv, *J. CO2 Util.*, 2019, **34**, 543–557.

9 P. Zhao, G. Zhang, Y. Sun and Y. Xu, *ENERG FUEL*, 2017, **31**, 12508–12520.

10 E. Niyonsenga, M. Wang, B. Wang, P. Liu, Y. Cao, H. Jin, S. Chen, Q. Teng, Q. Meng and N. Jia, *Appl. Surf. Sci.*, 2025, **707**, 163639.

11 X. Shen, F. Yan, Z. Zeng, P. Wang, F. Xie, X. Sun, H. Chen and Z. Zhang, *J. Mater. Chem. A*, 2024, **12**, 2697–2707.

12 S. Wang, X. Qiu, Y. Chen and S. Chen, *Micropor. Mesopor. Mat.*, 2022, **330**, 111585.

13 X. Chen, J. Lin, H. Wang, Y. Yang, C. Wang, Q. Sun, X. Shen and Y. Li, *Carbohydr. Polym.*, 2023, **302**, 120389.

14 S. Sepahvand, M. Jonoobi, A. Ashori, F. Gauvin, H. J. H. Brouwers, K. Oksman and Q. Yu, *Carbohydr. Polym.*, 2020, **230**, 115571.

15 C. Wang and S. Okubayashi, *Carbohydr. Polym.*, 2019, **225**, 115248.